

An *In Silico* Approach to Explicate the Binding Ability, Stability, and Reactivity of Bioactive Compounds from *Withania somnifera* as an ATP7A Regulator against Menke's Disease

Azar Zochedh ¹ , Shruthi Sundaram ¹, Kaliraj Chandran ¹ , Sureba Sukumaran ¹ ,
Thimma Mohan Viswanathan ¹ , Asath Bahadur Sultan ^{2,*} , Thandavarayan Kathiresan ^{1,*} 

¹ Department of Biotechnology, Kalasalingam Academy of Research and Education, Krishnankoil, Tamil Nadu, India

² Condensed Matter Physics Laboratory, Department of Physics, International Research Center, Kalasalingam Academy of Research and Education, Krishnankoil, Tamil Nadu, India

* Correspondence: s.asathbahadur@gmail.com (A.B.S.); t.kathiresan@klu.ac.in (T.K.);

Received: 3.05.2023; Accepted: 28.05.2023; Published: 5.09.2025

Abstract: Menkes disease (MD) is an X-linked, multisystemic, and lethal illness of copper metabolism. ATP7A, a protein that transports copper to secreted copper enzymes and is implicated in the export of extra copper from cells, is likely to be encoded by the faulty gene in MD (ATP7A). In this present study, sixty-nine bioactive phytochemicals from *Withania somnifera* were docked against the protein of the target ATP7A and screened based on their binding ability. The binding scores were observed from 2.6 Kcal/mol to -8.6 Kcal/mol. Then, screened top-hit phytochemicals were evaluated for drug-likeness characteristics, and all the top-hit phytochemicals exhibited fewer side effects and were predicted to be non-toxic. These top-hit compounds' stability and reactivity were further examined by employing frontier molecular orbitals with DFT/B3LYP on a 6-311G basis set. The phytochemicals' stability and reactivity were demonstrated by the detected energy gap, which ranged from 3.9766 eV to 6.7068 eV. The electrostatic potential map also revealed the distribution of charges among the atoms. This research will promote the use of *Withania somnifera* in conventional therapy and initiate the in vitro model to develop a novel medicine to treat Menke's disease.

Keywords: *Withania somnifera*; Menke's disease; molecular docking; HOMO-LUMO; ADMET; MEP.

© 2025 by the authors. This article is an open-access article distributed under the terms and conditions of the Creative Commons Attribution (CC BY) license (<https://creativecommons.org/licenses/by/4.0/>), which permits unrestricted use, distribution, and reproduction in any medium, provided the original work is properly cited. The authors retain copyright of their work, and no permission is required from the authors or the publisher to reuse or distribute this article, as long as proper attribution is given to the original source.

1. Introduction

Menkes disease (MD) is a multisystemic, fatal disorder of copper metabolism that is X-linked. Occipital horn syndrome (OHS) is the least severe of the component structures, and patients often have a devastating clinical history with early childhood mortality. The defective gene in MD (ATP7A) is expected to encode ATP7A, which transports copper to secreted copper enzymes and is involved in excess copper export from cells. The normal and unusual copper metabolism in humans and other organisms has been the focus of much investigation, and a wealth of data has been accumulated on this subject [1]. After iron and zinc, copper is the body's third-most abundant trace element, and it is required for the regular operation of

several copper enzymes involved in important metabolic activities. Dopamine b-hydroxylase, superoxide dismutase, peptidyl a-amidating enzyme, cell respiration, cytochrome-c oxidase (COX), elastin, collagen, keratin cross-linking, iron homeostasis, ceruloplasmin and hephaestin, and melanin production are all connected to copper. Copper is also involved in the biosynthesis of neurotransmitters (tyrosinase). Moreover, copper has been implicated in myelination under the control of the circadian cycle and may also be crucial for coagulation and angiogenesis. While being essential, a comparable metal may be very hazardous due to its chemical characteristics. Reversible interchange between these two states is the basis of enzymatic processes. Copper may exist in two oxidation states, Cu (I) and Cu (II). Yet, a related feature may result in the generation of free radicals, which have damaging effects on cellular components. Every living thing must thus adhere to the fine guidelines of copper homeostasis [2]. The primary aggravation in MD is the removal of copper from cells, and all tissues—aside from the liver and the brain—will collect copper to abnormally high levels. Although it is high, Maryland's copper concentration doesn't reach dangerous levels. Due to faulty copper export from the mucosal epithelium and usually decreased intestinal copper retention, together with metallothionein's scavenger role, these conditions exist. As ATP7B, not ATP7A, is the primary copper transporter in the normal liver, it is anticipated that the low copper level in the liver of MD patients will serve as a precondition for the metal in other organs [3]. The explanation for the reduced copper level in MD patients' brains is unusual in any case. One of the body's most lavishly copper-rich organs is the mammalian brain. While regulating brain copper levels isn't completely understood, ATP7A should be involved since MD causes low levels of copper in the brain. While the neurons and glial cells in MD patients are denied copper, copper is logically captured in the blood-brain and blood-cerebrospinal fluid barriers. This supports ATP7A's role in the uptake of copper in the brain. Due to ATP7A inactivation, MD patients also have neuronal demyelination [4]. It is suggested that ATP7A serves a purpose other than to hinder copper-dependent enzymes by intervening in ATP7A-related copper release through NMDA-receptor activation. So, it is likely that the neuronal degeneration and seizures that are seen in MD patients may also be linked to disturbed neuronal transmission caused by NMDA receptors that do not function properly [5].

The traditional Indian medical system of Ayurveda medicine extensively uses *Withania somnifera*, often known as ashwagandha. It is a component of many formulations recommended for a range of musculoskeletal diseases (such as arthritis and rheumatism) as well as a general tonic to boost energy, extend life, and enhance overall health in athletes, the elderly, and women during pregnancy [5,6]. Ashwagandha has been the subject of several pharmacological studies in an effort to confirm its efficacy as a multifaceted therapeutic agent [7,8]. For instance, investigations on its anti-inflammatory qualities have been done to support its usage in inflammatory arthritis, and studies on animal stress have been done to research its potential as an antistress drug [9,10]. Several research works have looked at the radiosensitizing and anticancer effects of *Withania somnifera* [11]. The current investigation in this paper aims to identify the biologically active phytochemicals from the *Withania somnifera* plant against Menke's disorder by targeting Copper-transporting ATPase, ATP7A. The investigation was performed through molecular modeling approaches like molecular docking, density functional theory, and pharmacokinetic analysis. Initially, all the bioactive compounds were analyzed for their binding affinity with the target protein, and then the top hit compounds were assessed for their structural stability and reactivity with DFT/B3LYP in a 6-311 G basis set. Finally, the top-hit molecules were assessed for drug-like features based on their

pharmacokinetic characteristics. These *in silico* findings will be useful for *in vitro* and *in vivo* studies of *Withania somnifera* plant against the ATP7A target for the treatment of Menke's disorder.

2. Materials and Methods

2.1. Graph theory network analysis.

The functional partners of the protein ATP7A in *Homo sapiens* were selected to determine the important protein network. The graph theoretical network analysis was produced using Cytoscape 3.9.1 and STRING (functional protein association network). The *homo sapiens* category in the STRING web server was used to look for the target protein ATP7A. The Cytoscape-specified CSV file was then exported from the findings that were created. The exported table was then placed into the Cytoscape graphical window, where the number of edges, nodes, and the whole network was evaluated [12].

2.2. Repossession and processing of protein structure.

The crystallographic structure of the target protein Copper-transporting ATPase, ATP7A (PDB ID: 7LU8), was retrieved from the online database RCSB PDB (<http://www.rcsb.org/pdb>) [13]. Prior to docking, the target proteins' structures were refined using the visualization tool BIOVIA Discovery Studio 2021 client. By including the missing residues and eliminating the existing ligands, atoms, and water molecules from the structure of ATP7A, the target proteins' structures were improved and stored in PDB format for further research.

2.3. Identification of active site.

The active site, sometimes called the binding site, on the target protein is a particular area where the ligand may attach and carry out a reaction. Through the use of the online CASTp (Computed Atlas of Surface Topography of Proteins) server, the target protein ATP7A active site was discovered (<http://sts.bioe.uic.edu/castp/index.html?3trg>) [14]. This tool helps us comprehend all data on the target protein's optimal chains as well as all active areas. It uses the PDB ID or Job ID when uploading a ready target structure. The target structure's total area and the number of active areas were used to choose the best pocket out of the many that emerged throughout processing.

2.4. Screening and retrieval of bioactive molecules.

Around sixty-nine bioactive compounds were analyzed from the selected plant, *Withania somnifera*, through the online tool IMPAAT (Indian Medicinal Plants, Phytochemistry and Therapeutics), a curated database (<https://cb.imsc.res.in/imppat/>) [15]. Then, the three-dimensional structure of these eighteen bioactive constituents was retrieved from the PubChem online database (<https://pubchem.ncbi.nlm.nih.gov/>) [16]. The structures were repossessed in .sdf format from PubChem for further validation and analysis.

2.5. Molecular docking simulation and visualization.

The computational method of molecular docking is widely used in the process of creating novel medications. The Python-based program PyRx 0.8 was used to conduct the docking analysis [17]. The ligand molecules were first imported into the workspace, and their energies were reduced. All ligands were then converted to PDBQT format. The target protein ATP7A (PDB ID: 7LU8) was then imported onto the PyRx tool's graphical display. Following the construction of the grid box at the target proteins' active areas, docking was carried out. Once the docking was complete, the program BIOVIA Discovery Studio was used to display the protein-ligand interactions. The PyRx output was provided as input in this. Analysis was done on the type of interaction, the bond category of interaction, and the separation between each interacted bond. The top hit phytochemicals against the target proteins were captured in 2-dimensional interactions using this technique.

2.6. Drug-likeness profile.

Drug development and identification depend heavily on pharmacokinetic (absorption, distribution, metabolism, and excretion) and physicochemical features. It is crucial to predict the safety or hazardous profile of suggested bioactive phytochemicals using small-molecule toxicology before such compounds are employed physiologically. The top hit compounds' canonical SMILES were retrieved from PubChem and used as an input file for the study. Through the use of the pKCSM program, the top-hit phytochemicals' physicochemical and ADMET properties were predicted (<https://biosig.lab.uq.edu.au/pkcsm/prediction>) [18].

2.7. Quantum chemical computation.

The Gaussian 09 program was used to do the quantum chemical computation [19]. The density function theory using the B3LYP/6-311G basis set. Using the DFT-B3LYP/6-311G basis set and Gaussian 09 software, the top hit compounds' 3D structures were optimized. The structural stability and reactivity of the optimized structure were then determined using frontier molecular orbital and molecular electrostatic potential studies. Gauss View 05 software was used to visualize the HOMO (highest occupied molecular orbital) and LUMO (lowest unoccupied molecular orbital) regions as well as the surface map of electrostatic potential [20].

3. Results and Discussion

3.1. Graph theory network analysis.

A graph illustrating the ATP7A pathway's network was created using the STRING and Cytoscape programs [21]. Figure 1 shows the correlations between several functional partner protein entities in the current investigation. The network has 11 nodes and 32 edges as determined by centrality traits, including betweenness, eccentricity, closeness, degree, stress, and radiality. The key functional members were appraised as Copper transport protein (ATOX1), Eukaryotic translation initiation factor 4 gamma 1 (EIF4G1), Extracellular superoxide dismutase (SOD3), PdZ domain-containing protein 11 (PDZD11), Glutaredoxin-1 (GLRX), High affinity copper uptake protein 1 (SLC31A1), Copper chaperone for superoxide dismutase (CCS), Ceruloplasmin (CP), Cytochrome c oxidase copper chaperone (COX17), and Probable low affinity copper uptake protein 2 (SLC31A2), respectively.

The assessed statistics exhibited that the network of ATP7A possesses eleven nodes, thirty-two edges, 5.818 average number of neighbors, a network diameter and radius of two and one, 1.418 characteristic path length, 0.784 clustering coefficient, 0.582 network density, 0.462 heterogeneity of network, and 0.511 of network centralization. The assessed centrality values of the ATP7A network are represented in Table 1. The higher results were obtained in all centrality measures for ATP7A. The assessed values of ATP7A for the degree were ten, betweenness was 0.327407, closeness and radiality were one, and stress was forty-six. Based on the determined results of centrality values, the protein Copper-transporting ATPase, ATP7A, was nominated as a potent target for Menke's disease, and this target was further utilized in molecular docking studies.

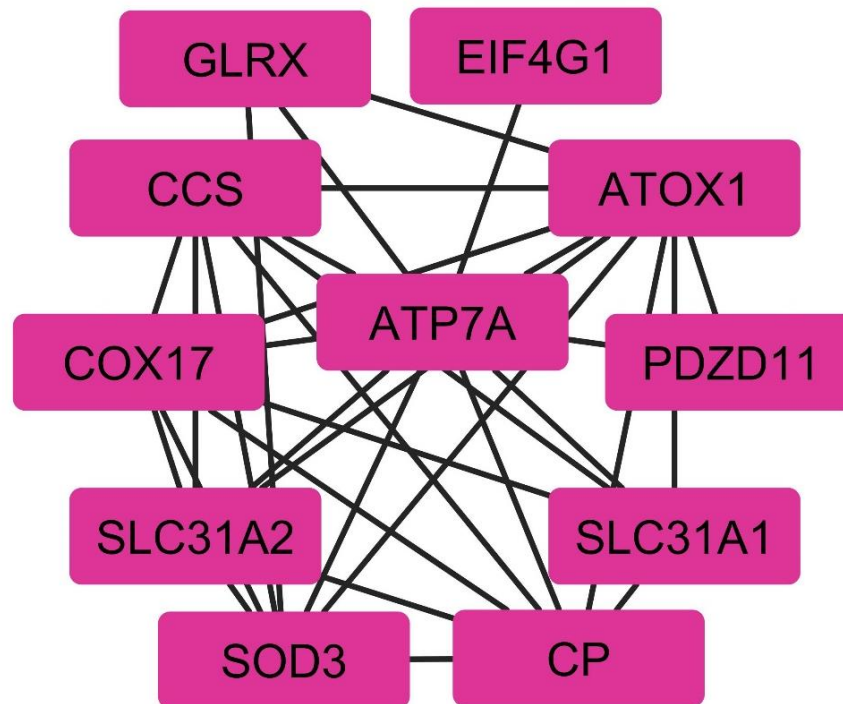


Figure 1. Graph theory network of the ATP7A pathway.

Table 1. The assessed threshold values of the ATP7A network.

Centrality measures	Degree	Betweenness	Closeness	Radiality	Stress
ATOX1	9	0.127407	0.909091	0.99	28
PDZD11	2	0	0.555556	0.92	0
SLC31A2	6	0	0.714286	0.96	0
COX17	7	0.008889	0.769231	0.97	4
CP	7	0.008889	0.769231	0.97	4
ATP7A	10	0.327407	1	1	46
SLC31A1	5	0	0.666667	0.95	0
GLRX	3	0	0.588235	0.93	0
SOD3	7	0.02963	0.769231	0.97	8
CCS	7	0.008889	0.769231	0.97	4
EIF4G1	1	0	0.526316	0.91	0

3.2. Active site prediction.

Through the CASTp v3.0 algorithm, active regions of the target protein ATP7A were predicted. The target ATP7A has 15 active pockets, according to the CASTp investigation. Among all active regions, the most noticeable optimal active zone should have the largest surface area and volume [22]. Despite having determined that ATP7A's active site regions were already known, the CASTp's top scores helped to cover additional potential pockets in the target protein's active regions. It has a bigger surface area of 277.784 Å² and a volume of

266.414 Å³. The number of appropriate pockets that are present in the target protein's active regions is revealed by CASTp results. The target protein ATP7A's residues were examined to determine which ones were in the active regions. One of the ATP7A's predicted active pockets was chosen as an active region as shown in Figure 2, and it comprises the following residues ASP6, THR7, LEU8, PHE9, LEU10, VAL47, ILE49, PRO51, VAL54, ASN55, ALA56, ASN57, ILE59, LYS60, SER67, LEU68, THR72, LEU73, GLU74, LYS75 and LYS76. These residues were chosen and used for selective docking, enabling analysis of the interaction profile. These ATP7A target protein active site regions were employed during the molecular docking procedure. A grid box was made in the target protein using these active site regions to enable ligand binding. Increased binding affinity and better docking results for ligands may result from docking in active regions.

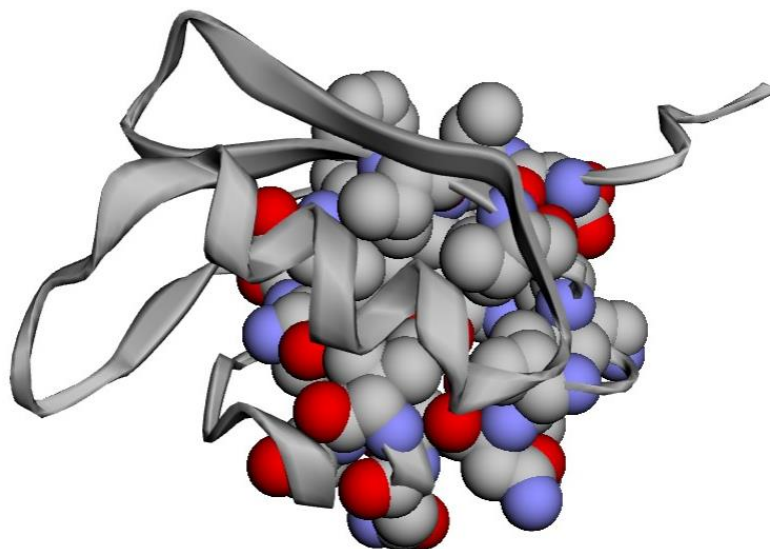


Figure 2. Predicted active surface area of the target protein ATP7A through CASTp.

3.3. Molecular docking analysis.

The ability of the bioactive phytochemicals contained in *Withania somnifera* to bind to the target protein's receptor region was examined using molecular docking [23]. The sixty-nine bioactive phytochemicals from *Withania somnifera* were chosen for the molecular docking investigation toward the target protein ATP7A (PDB ID: 7LU8). Molecular docking was performed through PyRx software. From the results of docking files, the binding affinity of sixty-seven bioactive compounds was found to be scattered from the range of -2.6 to -8.6 kcal/mol. Table 2 represents the list of sixty-seven bioactive compounds showing significant binding energy with ATP7A (PDB ID: 7LU8). The phytochemical choline (CID: 305) exhibits the lowest binding energy (-2.6 kcal/mol), whereas the phytochemical 27-deoxywithaferin (CID: 23266155) exhibits the highest binding energy (-8.6 kcal/mol) with the target protein. Eight bioactive compounds were found to have high binding energies (≤ -8 kcal/mol) with ATP7A. The top eight bioactive compounds are 27-deoxywithaferin (CID: 23266155), coagulin q (CID: 162623730), physagulin-d (CID: 10100412), sitoindoside IX (CID: 189586), solasodine (CID: 442985), somniferine (CID: 14106343), stigmaterol glucoside (CID: 6602508) and withanolide (CID: 53477765) with the binding energy of -8.3, -8.6, -8.4, -8.2, -8, -8.1, -8 and -8.5 kcal/mol respectively. These compounds were designated for future estimation based on their binding energy with the target protein.

Table 2. Binding ability of bioactive compounds from *W. somnifera* against ATP7A.

PubChem CID	Bioactive compounds	Binding affinity (Kcal/mol)
443143	(-)-Anaferrine	-4.9
70684083	2,3-dehydrosomnifericin	-7.7
157009865	2,4-methylene-cholesterol	-6.8
15411208	2-3-dihydrowithaferin	-7.5
73621	4-beta-hydroxywithanolide	-7.2
13743195	4-deoxyphysalolactone	-7.2
58427569	4-o-caffeoylquinic-acid	-6
44423097	17-alpha-hydroxywithanolide	-7.7
21679024	17-isowithanolide e	-7.3
6428670	24-Methyl-5-alpha-cholesta-8,24(28)-dien-3-beta-ol	-6.7
5283652	24-methylcholesta-5,23E-dien-3beta-ol	-7.2
193567	24-methyl-desmosterol	-7.3
23266158	27-Deoxy-14-hydroxywithaferin A	-7.4
23266155	27-deoxywithaferin	-8.6
12306778	Anahygrine	-4.8
73145	Beta-Amyrin	-7
222284	Beta-sitosterol	-6.8
173183	Campesterol	-6.8
1794427	Chlorogenic-acid	-6.4
305	Choline	-2.6
162623730	Coagulin Q	-8.4
1201543	Cuscohygrine	-4.5
5862	Cysteine	-3.3
67678	Cystine	-3.4
5742590	Daucosterol	-7.5
11850	Dulcitol	-3.9
444679	Ergosterol	-7.1
5281416	Esculetin	-5.2
5281328	Fucosterol	-7.2
119	Gamma-Aminobutyric acid	-3.2
12410	Hentriacontane	-4.7
16623	Hydrocortisone sodium succinate	-6.1
5810	Hydroxyproline	-4
440933	Hygrine	-3.6
6474309	Isochlorogenic-acid-c	-6.2
92987	Isopelletierine	-4.1
5280450	Linoleic-acid	-5.3
11005	Myristic acid	-4.8
89594	Nicotine	-4.4
12408	Octacosane	-4.7
10494	Oleanolic acid	-6.5
445639	Oleic acid	-4.3
985	Palmitic acid	-4.2
92987	Pelletierine	-4.1
10100412	Physagulin-d	-8.2
449293	Pseudotropine	-3.7
5280343	Quercetin	-6.2
6508	Quinic-acid	-4.5
5280460	Scopoletin	-5
189586	Sitoindoside IX	-8
442985	Solasodine	-8.3
44249449	Sominone	-7.7
102066415	Somniferanolide	-7.8
101687980	Somnifericin	-7.7
14106343	Somniferine	-8.1
102066417	Somniwithanolide	-7.4
5281	Stearic-acid	-4.6
6602508	Stigmasterol glucoside	-8
5280794	Stigmasterol	-7.2
8424	Tropine	-3.7
57403080	Viscosalactone B	-7.7
12444955	Withanicandrin	-7.9
21679022	Withanolide J	-7.6
53477765	Withanolide	-8.5
21679027	Withanone	-7.8

PubChem CID	Bioactive compounds	Binding affinity (Kcal/mol)
101687981	Withaoylactone	-7.3
442877	Withasomnine	-5.4

3.4. Analysis of protein-ligand interactions of top-hit phytochemicals.

The binding interactions of the top eight bioactive compounds with target protein ATP7A (PDB ID: 7LU8) were visualized in BIOVIA Discovery Studio 2021. The bond type and bond distances were also analyzed [24]. The 3D and 2D interactions of the top eight bioactive compound complexes were studied and shown in Figure 3. It was observed that binding interaction of 27-deoxywithaferin with ATP7A forms twelve (12) alkyl bonds with residues LYS75 (3), PRO51 (3), VAL54, LEU8, ILE59 (2) and ALA56 (2) with a bond distance of 4.13914, 5.30467, 5.05887, 5.17166, 4.78071, 4.17367, 4.04296, 4.52215, 5.41479, 5.43413, 3.70958 and 4.35997 Å respectively. The binding interaction of Coagulin Q with ATP7A forms a conventional hydrogen bond with residues HIS3 at a distance of 2.19268 Å. It also forms a carbon-hydrogen bond and twelve (12) alkyl bonds with residues ASP6, LEU8, PRO51 (3), VAL54, ALA56 (2), ILE59 and LYS75 (4) at a distance of 2.589, 4.51748, 4.54544, 4.30342, 5.0443, 4.20052, 3.71098, 4.25458, 5.29712, 5.04238, 5.25931, 5.47794 and 4.47991 Å respectively. The interaction of Physagulin-d with ATP7A forms four (4) conventional hydrogen bonds with residues HIS3 (3) and ASP6 at a distance of 2.96693, 1.86316, 2.34098, and 2.33549 Å, respectively. It also forms four (4) carbon-hydrogen bonds and nine (9) with alkyl bonds ASP6 (2), HIS3, GLY2, LYS75 (3), PRO51 (3), VAL54, ALA56 and ILE59 at distance of 2.47923, 2.78733, 3.08674, 2.7855, 4.15916, 5.21589, 3.94976, 4.88452, 4.096, 4.72273, 4.18166, 4.19877 and 5.08712 Å respectively. The interaction of Sitoindoside IX with ATP7A forms two (2) conventional hydrogen bonds with LEU73 and GLU74 with distances of 1.81715 Å and 2.59721 Å. It also forms three (3) carbon-hydrogen and five (5) alkyl bonds with residues THR7, LUE73, THR72, PRO51 (2), ALA56, and LYS75 (2) with the bond distances of 2.38032, 2.82133, 2.38966, 4.07208, 4.70242, 4.17522, 4.33205, and 4.56792 Å, respectively. The interaction of Solasodine with ATP7A forms a carbon-hydrogen bond with residue LEU73 with a bond distance of 2.44083 Å. It also forms two (2) Pi-Alkyl bonds and six (6) alkyl bonds with residues PHE9 (2), LEU73 (2), LEU8 (2), and PRO51 (2) with bond distances of 4.6504, 4.90456, 4.93169, 5.04477, 4.50033, 4.75802, 4.38093, and 3.8847 Å, respectively. The interaction of Somniferine with ATP7A forms a carbon-hydrogen bond with residue ASN55 with a bond distance of 2.7014 Å. It forms Pi-Anion and three (3) alkyl bonds with residues GLU74, LEU8, PRO51, and ALA56 with bond distances of 3.56866, 4.38718, 4.98817, and 4.23646 Å, respectively. It also forms a Pi-alkyl bond with residue PRO51 with a bond distance of 4.50503 Å. The interaction of Stigmasterol glucoside with ATP7A forms three (3) conventional hydrogen bonds with residues HIS3 (3) with a bond distance of 2.11835, 2.33899, 2.64936 Å. It forms four (4) carbon hydrogen and twelve (12) alkyl bonds with residues HIS3, GLY2 ASP6 (2), LEU8 (2), ILE59, PRO51 (3), ALA56 (2) and LYS75 (4) with a bond distance of 2.87944, 2.54971, 2.77319, 2.92161, 4.73899, 5.22063, 5.18837, 4.72518, 4.06064, 4.86474, 3.76847, 3.52693, 4.32793, 5.46328, 5.20749 and 3.98306 Å respectively. The interaction of withanolide with ATP7A forms eleven (11) alkyl bonds with residue LEU8, PRO51(3), VAL54, ALA56 (2), ILE59, and LYS75(3) with bond distances 4.48002, 5.10011, 4.77395, 4.17352, 4.07022, 3.74592, 4.35106, 5.42877, 4.16632, 5.39208, and 5.09399 Å respectively. The category of bond interaction, bond length, and donor and acceptor domains of the hydrogen bond are used in the molecular docking simulation to display the top-hit compound's ability to attach to the target protein at its active

receptor sites [25–27]. These eight bioactive phytochemicals of *W. somnifera* have the advantages of potent binding capacity, strong hydrogen bond interactions, and another bond binding to the amino acids that occur at the active sites of the desired protein [28]. This makes them potent therapeutic agents for the treatment of Menke's disease.

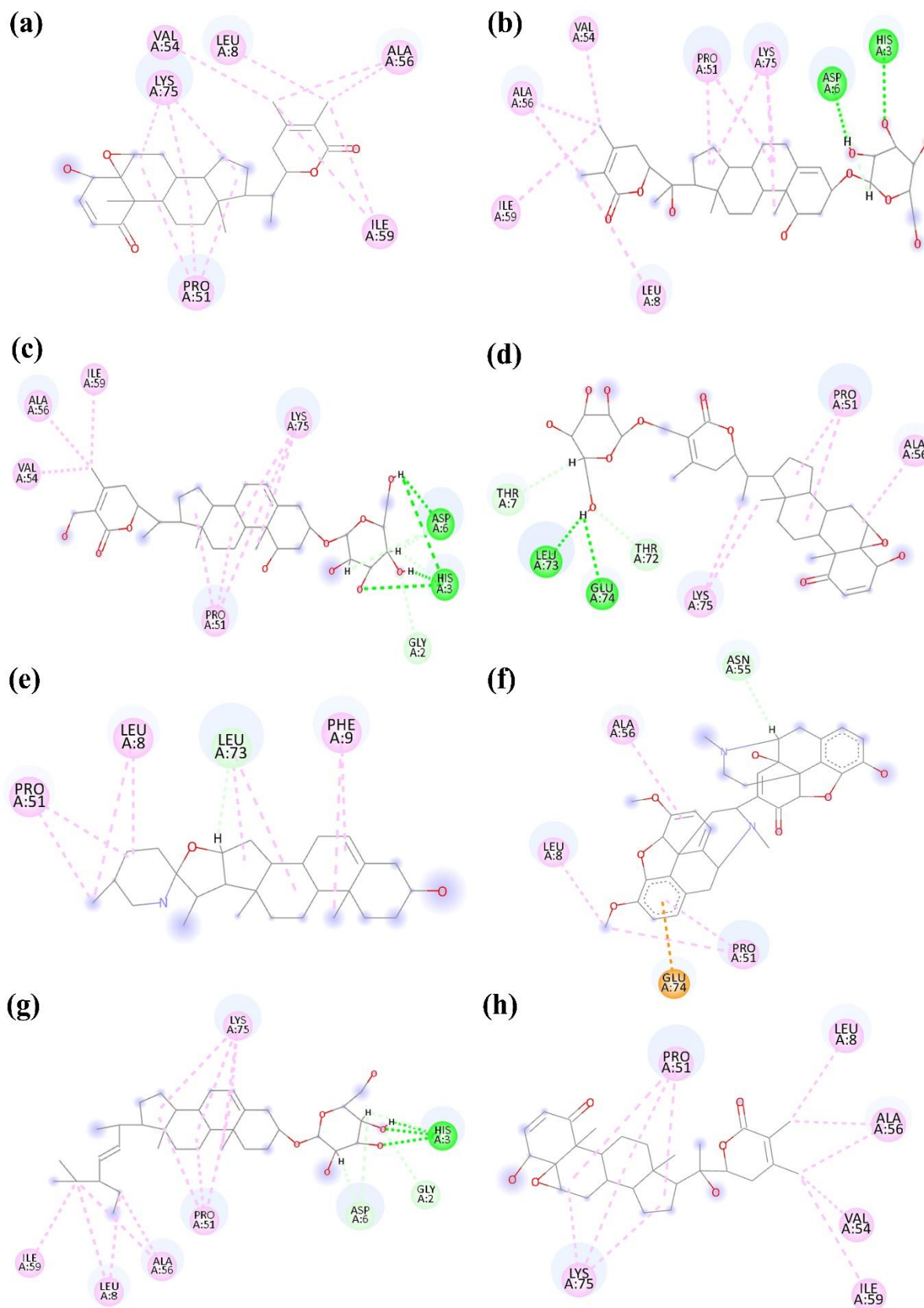


Figure 3. 2-dimensional interactions of the top eight phytochemicals with the target protein ATP7A, with their bond category. (a) 27-deoxywithaferin; (b) coagulin Q; (c) physagulin-d; (d) sitoindoside IX; (e) solasodine; (f) somniferine; (g) stigmasterol glucoside; (h) withanolide.

3.5. Drug-likeness assessment.

The absorption, distribution, metabolism, excretion, and toxicity analysis for best-docked bioactive compounds were predicted through the online software tool pkCSM [29]. The data in Table 3 represent the ADMET properties of selected bioactive compounds. It was observed that the bioactive compound somniferine exhibits the highest water solubility of -3.120, and 27-deoxywithaferin exhibits the least water solubility of -5.418. Caco2 permeability values were accounted for between the range of 1.530 and 0.192. The compound somniferine possesses the highest Caco2 permeability, whereas coagulin q shows the least permeability. Intestinal absorption of withanolide shows 99.2%, which means it can be easily absorbed by human intestinal cells. The skin permeability value of these compounds ranged from -2.736 to -3.267. The phytochemical somniferine possesses the highest permeability, followed by physagulin-d and withanolide, which possess the least permeability. All the bioactive compounds except 27-deoxywithaferin are P-glycoprotein substrates. All the bioactive compounds are P-glycoprotein I inhibitors. Except coagulin q, physagulin-d, and sitoindoside IX; all selected bioactive compounds are P-glycoprotein II inhibitors. The steady-state volume distribution (VD_{ss}) was relatively low for all the bioactive compounds other than somniferine. Somniferine showed a VD_{ss} value of 1.633, and coagulin q showed a low VD_{ss} with a value of -1.204. Solasodine crosses the blood-brain barrier, and other bioactive compounds poorly cross through it. The phytochemicals 27-deoxywithaferin and withanolide readily penetrate the CNS, and the remaining phytochemicals were found with a range less than -3; therefore, they cannot penetrate the CNS. None of the phytochemicals were CYP2D6 substrates, CYP1A2 inhibitors, CYP2C19 inhibitors, CYP2C9 inhibitors, or CYP2D6 inhibitors. Except physagulin-d; all other phytochemicals were CYP3A4 substrates. Only somniferine was the inhibitor of CYP3A4. Somniferine is the highest, and solasodine has the lowest total clearance values of 1.051 and 0.09, respectively. None of the selected bioactive compounds were renal OCT2 substrates. All top eight phytochemicals show no toxicity for the AMES parameter. Solasodine shows the highest tolerated dosage in humans, with a value of -0.375, and sitoindoside IX shows the lowest tolerated dosage with a value of -1.936. None of the phytochemicals were hERG I inhibitors. Except 27-deoxywithaferin, withanolide, and stigmaterol glucoside; all other phytochemicals were hERG II inhibitors. The LD₅₀ values of phytochemicals: 27-deoxywithaferin, withanolide, coagulin q, solasodine, physagulin-d, somniferine, stigmaterol glucoside, and sitoindoside IX are 2.421, 2.831, 2.736, 2.489, 2.773, 3.111, 2.572, and 3.891, and LOAEL values were -0.038, 1.776, 2.641, 1.332, 3.416, 1.384, 3.315, and 2.862 respectively. Except for solasodine, no other phytochemical shows hepatotoxicity. The selected phytochemicals show no skin sensitization. These ADMET parameters exhibited the drug-likeness features of the top eight phytochemicals with no toxicity and side effects [30]. Therefore, these top-hit phytochemicals can be further utilized as oral drugs after clinical validation.

Table 3. Physicochemical and Pharmacokinetic properties of the top eight phytochemicals.

Descriptor	27-deoxywithaferin	Withanolide	Coagulin Q	Solasodine	Physagulin-d	Somniferine	Stigmaterol glucoside	Sitoindoside IX
Water solubility (log mol/L)	-5.418	-5.127	-4.330	-3.809	-3.959	-3.120	-4.714	-4.419
Caco2 permeability (log Papp)	0.800	0.831	0.192	1.292	0.429	1.530	0.493	0.412

Descriptor	27-deoxywithaferin	Withanolide	Coagulin Q	Solasodine	Physagulin-d	Somniferine	Stigmasterol glucoside	Sitoindoside IX
Human Intestinal absorption (%)	97.390	99.200	51.990	92.324	54.898	94.052	78.899	55.154
Skin permeability (log Kp)	-3.246	-3.267	-2.754	-3.230	-2.737	-2.736	-2.750	-2.738
P-glycoprotein substrate	No	Yes	Yes	Yes	Yes	Yes	Yes	Yes
P-glycoprotein I inhibitor	Yes	Yes	Yes	Yes	Yes	Yes	Yes	Yes
P-glycoprotein II inhibitor	Yes	Yes	No	Yes	No	Yes	Yes	No
VDss (human)	0.057	-0.048	-1.204	0.324	-0.813	1.633	-1.162	-0.626
Fraction unbound (human)	0.010	0.093	0.269	0.195	0.292	0.262	0.078	0.317
BBB permeability	-0.155	-0.315	-1.120	0.035	-1.066	-0.548	-0.724	-1.183
CNS permeability	-1.813	-2.696	-3.506	-3.047	-3.532	-3.073	-3.002	-3.703
CYP2D6 substrate	No	No	No	No	No	No	No	No
CYP3A4 substrate	Yes	Yes	Yes	Yes	No	Yes	Yes	Yes
CYP1A2 inhibitor	No	No	No	No	No	No	No	No
CYP2C19 inhibitor	No	No	No	No	No	No	No	No
CYP2C9 inhibitor	No	No	No	No	No	No	No	No
CYP2D6 inhibitor	No	No	No	No	No	No	No	No
CYP3A4 inhibitor	No	No	No	No	No	Yes	No	No
Total clearance	0.364	0.347	0.528	0.09	0.615	1.051	0.674	0.459
Renal OCT2 substrate	No	No	No	No	No	No	No	No
AMES toxicity	No	No	No	No	No	No	No	No
Max. tolerated dose (human)	-0.557	-0.867	-1.509	-0.375	-1.727	-0.873	-0.908	-1.936
hERG I inhibitor	No	No	No	No	No	No	No	No
hERG II inhibitor	No	No	Yes	Yes	Yes	Yes	No	Yes
Oral Rate acute toxicity (LD50)	2.421	2.831	2.736	2.489	2.773	3.111	2.572	3.891
Oral Rat Chronic Toxicity (LOAEL)	-0.038	1.776	2.641	1.332	3.416	1.384	3.315	2.862
Hepatotoxicity	No	No	No	Yes	No	No	No	No
Skin Sensitisation	No	No	No	No	No	No	No	No

3.6. Frontier molecular orbital analysis.

Understanding the frontier molecular orbitals (FMOs) is essential because of their significant influence on how reactive each individual molecule behaves. The highest occupied molecular orbital (HOMO) and lowest unoccupied molecular orbital (LUMO) are used to study how molecules interact with other objects [31, 32]. The HOMO and LUMO energies describe the capacity to give and accept electrons. As chemical reactions occur, interactions between HOMO and LUMO in reacting species are crucial for stabilizing the transition structure. The HOMO-LUMO energy gap values of any molecular system may be utilized to describe the kinetic stability and chemical reactivity of a system of molecules [33]. The well-known

softness-hardness rule states that a material's thermal and kinetic stability and energy gap increase with increasing hardness. Soft molecules with high chemical reactivity and low kinetic stability are usually linked with small HOMO-LUMO gaps [34]. The calculated HOMO, LUMO, and energy gap values of the top hit compounds were tabulated in Table 4. The calculated LUMO values of 27-deoxywithaferin, Withanolide, Coagulin Q, Solasodine, Physagulin-d, Somniferine, Stigmasterol glucoside, and Sitoindoside IX were 1.0814 eV, 1.1347 eV, 1.7940 eV, 3.5345 eV, 1.8030 eV, 1.0359 eV, 3.5184 eV and 1.0153 eV, whereas the HOMO values were -3.5405 eV, -3.4904 eV, -3.2624 eV, -3.0735 eV, -3.2352 eV, -2.9407 eV, -3.1884 eV and -3.4058 eV. The difference between these HOMO and LUMO energies was calculated to determine the band gap. The energy band gap was calculated by the equation $\Delta E = ELUMO - EHOMO$. Based on the calculated values of the band gap, the kinetic stability and chemical reactivity of each phytochemical were analyzed. The energy gap of the phytochemicals falls between the range of 3.9766 eV and 6.7068 eV. The lowest energy gap was observed for the phytochemical Somniferine, which shows good chemical reactivity and lesser stability of structure. The highest energy gap value was with phytochemical Stigmasterol glucoside, which confirms better kinetic stability and less chemical reactivity.

Table 4. Calculated HOMO, LUMO, and energy band gap values of the top eight phytochemicals.

S. No	Phytochemicals	LUMO (eV)	HOMO (eV)	ΔE (eV)
1.	27-deoxywithaferin	1.0814	-3.5405	4.6219
2.	Withanolide	1.1347	-3.4904	4.6251
3.	Coagulin Q	1.7940	-3.2624	5.0564
4.	Solasodine	3.5345	-3.0735	6.608
5.	Physagulin-d	1.8030	-3.2352	5.0382
6.	Somniferine	1.0359	-2.9407	3.9766
7.	Stigmasterol glucoside	3.5184	-3.1884	6.7068
8.	Sitoindoside IX	1.0153	-3.4058	4.4211

3.7. Molecular electrostatic potential.

The components' form, dimension, and electrostatic potential are frequently represented as molecular electrostatic potential in color grading. It's a fantastic tool for learning about a molecule's physical as well as chemical characteristics [35, 36]. For the eight top-hit organic substances 27-deoxywithaferin, Withanolide, Coagulin Q, Solasodine, Physagulin-d, Somniferine, Stigmasterol glucoside, and Sitoindoside IX that were investigated using DFT/B3LYP techniques at the 6-311 G basis set, an electrostatic potential map surface was created. The phytochemicals 27-deoxywithaferin, Withanolide, Coagulin Q, Solasodine, Physagulin-d, Somniferine, Stigmasterol glucoside, and Sitoindoside IX all have their molecular electrostatic potential surfaces shown in Figure 4.

The zone investigates and discusses nucleophilic and electrophilic properties in a different color spectrum. The color blue represents a higher nucleophilic potential, whereas the color red denotes a higher electrophilic potential. The electrical potential dips are described in the sequence below: blue, cyan, green, yellow, orange, and red [37, 38]. The color grade of 27-deoxywithaferin falls in the range of -6.291×10^{-2} to $+6.291 \times 10^{-2}$; for withanolide, the range was from -6.249×10^{-2} to $+6.249 \times 10^{-2}$; for coagulin Q, the range falls between -5.784×10^{-2} to $+5.784 \times 10^{-2}$, solasodine the range was -5.604×10^{-2} to $+5.604 \times 10^{-2}$, for Physagulin-d the color ranges from -6.346×10^{-2} to $+6.346 \times 10^{-2}$, Somniferine falls in the range of -7.771×10^{-2} to $+7.771 \times 10^{-2}$, Stigmasterol glucoside falls between the range of -6.420×10^{-2} to $+6.420 \times 10^{-2}$, and the phytochemical Sitoindoside IX possesses the color range from -5.711×10^{-2} to $+5.711 \times 10^{-2}$.

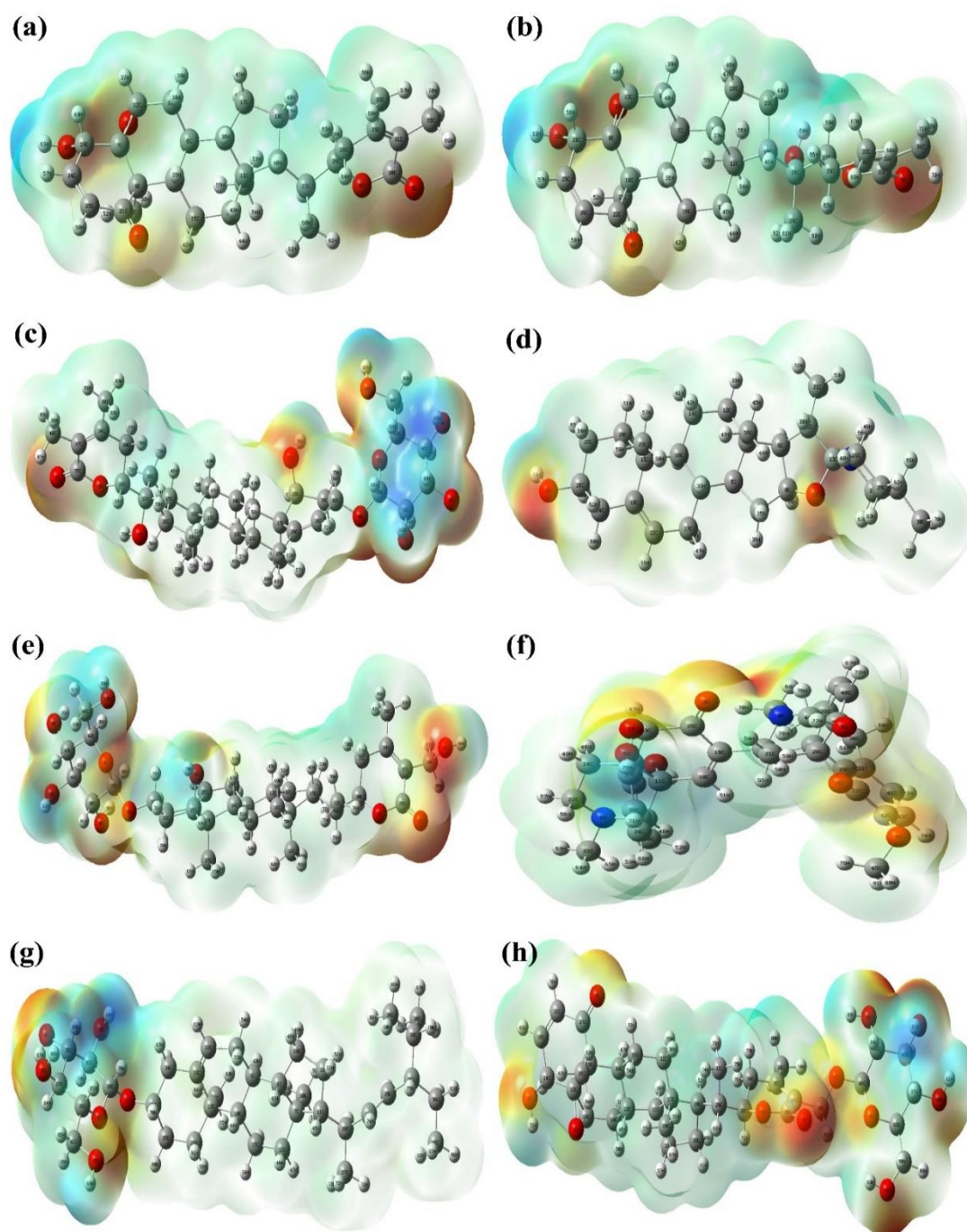


Figure 4. Molecular electrostatic potential map of the top eight phytochemicals. (a) 27-deoxywithaferin; (b) Withanolide; (c) Coagulin Q; (d) Solasodine; (e) Physagulin-d; (f) Somniferine; (g) Stigmasterol glucoside; (h) Sitoindoside IX.

Figure 4 exhibits that all oxygen atoms in the top eight phytochemicals were observed at the red surface of the electrostatic map, which confirms that the oxygen atoms fall in the electron-rich area, and the hydrogen and other carbon atoms were found in the blue or partially green regions, which are electron-poor areas. This demonstrates that all of the oxygen atoms in the top eight phytochemicals will form a hydrogen bond, improving their propensity to bind. All of these top-hit compounds showed a definite depolarization of the charge [39].

4. Conclusions

The findings of this study showed that all of the bioactive phytochemicals from *Withania somnifera* had the ability to bind to the active pockets of the target protein ATP7A,

indicating that these phytochemicals may be helpful in the treatment of Menke's disease. Eight phytochemicals, 27-deoxywithaferin, Withanolide, Coagulin Q, Solasodine, Physagulin-d, Somniferine, Stigmasterol glucoside, and Sitoindoside IX, showed more potent affinity than -8.0 Kcal/mol, according to the docking results. The potential of the top eight phytochemicals as oral drugs and drug-like qualities was demonstrated by physicochemical and ADME investigations. The safety profile and harmful effects of the top-hit compounds were revealed by the toxicology study. Frontier molecular orbitals were used to assess the molecular reactivity, kinetic stability, and intramolecular charge transfer of popular phytochemicals, and the energy difference between LUMO and HOMO revealed the stability and reactivity of the compounds. Through molecular electrostatic potential, each atom's atomic charges in compounds were assessed, and the charge depolarization was noticed. To fully comprehend the activities and efficacy of *W. somnifera* for the treatment of Menke's disease, more *in vivo* and *in vitro* research is necessary. The most effective phytochemicals were those that demonstrated greater binding affinity at the receptors of the target protein ATP7A, as a regulator of copper channels, and might be used as a strong medication to treat Menke's disease.

Author Contributions

All authors have read and agreed to the published version of the manuscript.

Institutional Review Board Statement

Not applicable.

Informed Consent Statement

Not applicable.

Data Availability Statement

Data supporting the findings of this study are available upon reasonable request from the corresponding author.

Funding

This research was funded by a Grant-aid from the Department of Biotechnology (DBT), Ministry of Science and Technology, India [BT/PR44695/NER/95/1880/2021].

Acknowledgments

The authors acknowledge Dr. S. Athimoolam, Department of Physics, University College of Engineering, Nagercoil, for helping us in utilizing the Gaussian 09 Program.

Conflicts of Interest

The authors declare no conflict of interest.

References

1. Bertini, I.; Rosato, A. Menkes disease. *Cellular and Molecular Life Sciences* **2008**, *65*, 89-91, <https://doi.org/10.1007/s00018-007-7439-6>.

2. Horn, N.; Tümer, Z. Menkes Disease and the Occipital Horn Syndrome. In *Connective Tissue and Its Heritable Disorders*, 2nd Edition; Royce, P.M., Steinmann, B., Eds.; Wiley–Blackwell: **2002**; pp. 651-685, <https://doi.org/10.1002/0471221929.ch14>.
3. Nishihara, E.; Furuyama, T.; Yamashita, S.; Mori, N. Expression of copper trafficking genes in the mouse brain. *Neuroreport* **1998**, *9*, 3259-3263, <https://doi.org/10.1097/00001756-199810050-00023>.
4. Liu, P. C.; Chen, Y. W.; Centeno, J. A.; Quezado, M.; Lem, K.; Kaler, S. G. Downregulation of myelination, energy, and translational genes in Menkes disease brain. *Molecular genetics and metabolism* **2005**, *85*, 291-300, <https://doi.org/10.1016/j.ymgme.2005.04.007>.
5. Schlieff, M.L.; Craig, A.M.; Gitlin, J.D. NMDA receptor activation mediates copper homeostasis in hippocampal neurons. *Journal of Neuroscience* **2005**, *25*, 239-246, <https://doi.org/10.1523/JNEUROSCI.3699-04.2005>.
6. Chatterjee, A.; Pakrashi, S.C. Treatise on Indian medicinal plants, vol III. *Publications and Information Directorate, CSIR, New Delhi*, **1995**, *5*, 60-71.
7. Bone, K. Clinical applications of Ayurvedic and Chinese herbs. Phytotherapy Press, Queensland, Australia, **1996**, *13*, 7-41.
8. Anbalagan, K.; Sadique, J. Influence of an Indian medicine (Ashwagandha) on acute-phase reactants in inflammation. *Indian journal of experimental biology* **1981**, *19*, 245-249.
9. Archana, R.; Namasivayam, A. Antistressor effect of Withania somnifera. *Journal of ethnopharmacology* **1998**, *64*, 91-93, [https://doi.org/10.1016/S0378-8741\(98\)00107-X](https://doi.org/10.1016/S0378-8741(98)00107-X).
10. Dhuley, J. N. Effect of ashwagandha on lipid peroxidation in stress-induced animals. *Journal of ethnopharmacology* **1998**, *60*, 173-178, [https://doi.org/10.1016/S0378-8741\(97\)00151-7](https://doi.org/10.1016/S0378-8741(97)00151-7).
11. Devi, P. U.; Sharada, A. C.; Solomon, F. E.; Kamath, M. S. In vivo growth inhibitory effect of Withania somnifera (Ashwagandha) on a transplantable mouse tumor, Sarcoma 180. *Indian journal of experimental biology* **1992**, *30*, 169-172.
12. Saravanan, G.; Panneerselvam, T.; Kunjiappan, S.; Parasuraman, P.; Alagarsamy, V.; Udayakumar, P.; Ammunje, D. N. Graph theoretical analysis, in silico modeling, prediction of toxicity, metabolism and synthesis of novel 2-(methyl/phenyl)-3-(4-(5-substituted-1, 3, 4-oxadiazol-2-yl) phenyl) quinazolin-4 (3H)-ones as NMDA receptor inhibitor. *Drug Development Research* **2019**, *80*, 368-385, <https://doi.org/10.1002/ddr.21511>.
13. Berman, H. M.; Westbrook, J.; Feng, Z.; Gilliland, G.; Bhat, T. N.; Weissig, H.; Bourne, P. E. The protein data bank. *Nucleic acids research* **2000**, *28*, 235-242, <https://doi.org/10.1093/nar/28.1.235>.
14. Tian, W.; Chen, C.; Lei, X.; Zhao, J.; Liang, J. CASTp 3.0: computed atlas of surface topography of proteins. *Nucleic acids research* **2018**, *46*, W363-W367, <https://doi.org/10.1093/nar/gky473>.
15. Vivek-Ananth, R. P.; Mohanraj, K.; Sahoo, A. K.; Samal, A. IMPPAT 2.0: an enhanced and expanded phytochemical atlas of Indian medicinal plants. *ACS omega* **2023**, *8*, 8827-8845, <https://doi.org/10.1021/acsomega.3c00156>.
16. Kim, S.; Thiessen, P. A.; Bolton, E. E.; Chen, J.; Fu, G.; Gindulyte, A.; Bryant, S. H. PubChem substance and compound databases. *Nucleic acids research* **2016**, *44*, D1202-D1213, <https://doi.org/10.1093/nar/gkv951>.
17. Dallakyan, S.; Olson, A.J. Small-Molecule Library Screening by Docking with PyRx. In *Chemical Biology: Methods and Protocols*, Hempel, J.E., Williams, C.H., Hong, C.C., Eds.; Springer New York: New York, NY, **2015**; Volume 1263, pp. 243-250, https://doi.org/10.1007/978-1-4939-2269-7_19.
18. Pires, D. E.; Blundell, T. L.; Ascher, D. B. pkCSM: predicting small-molecule pharmacokinetic and toxicity properties using graph-based signatures. *Journal of medicinal chemistry* **2015**, *58*, 4066-4072, <https://doi.org/10.1021/acs.jmedchem.5b00104>.
19. Frisch, A. gaussian 09W Reference. *Wallingford, USA*, **2009**, *25p*, 470.
20. Dennington, R.; Keith, T.; Millam, J. GaussView, version 5, Semicem Inc., Shawnee Mission: **2009**.
21. Szklarczyk, D.; Gable, A. L.; Nastou, K. C.; Lyon, D.; Kirsch, R.; Pyysalo, S.; von Mering, C. The STRING database in 2021: customizable protein–protein networks, and functional characterization of user-uploaded gene/measurement sets. *Nucleic acids research* **2021**, *49*, D605-D612, <https://doi.org/10.1093/nar/gkaa1074>.
22. Zochedh, A.; Priya, M.; Chakaravarthy, C.; Sultan, A. B.; Kathiresan, T. Experimental and Computational Evaluation of Syringic Acid–Structural, Spectroscopic, Biological Activity and Docking Simulation. *Polycyclic Aromatic Compounds* **2022**, *43*, 1-33, <https://doi.org/10.1080/10406638.2022.2118332>.
23. Zochedh, A.; Priya, M.; Shunmuganarayanan, A.; Sultan, A. B.; Kathiresan, T. Antitumor and antimicrobial effect of syringic acid urea cocrystal: Structural and spectroscopic characterization, DFT calculation and

- biological evaluation. *Journal of Molecular Structure* **2023**, *1282*, 135113, <https://doi.org/10.1016/j.molstruc.2023.135113>.
24. Sharmili Banu, K. R.; Mohana Priya, I.; Azar Zochedh, A. S. Identification of novel bioactive compounds from banana fruit (*Musa sapientum*) as antidepressant in pregnant women: molecular docking, physicochemical and ADMET evaluation. *Asian Journal of Biotechnology and Genetic Engineering* **2022**, *5*, 9-24.
 25. Zochedh, A. A.; Bahadur, S. A.; Kathiresan, T. Quantum chemical and molecular docking studies of naringin: a potent anticancer drug. *Journal of Cardiovascular Disease Research* **2021**, *12*, 1140-1148.
 26. Zochedh, A.; Chandran, K.; Priya, M.; Sultan, A. B.; Kathiresan, T. DFT Simulation of Berberine Chloride with Spectroscopic Characterization–Biological activity and Molecular Docking against Breast Cancer. *Polycyclic Aromatic Compounds* **2023**, *43*, 1-25, <https://doi.org/10.1080/10406638.2023.2201457>.
 27. Asiamah, I.; Obiri, S. A.; Tamekloe, W.; Armah, F. A.; Borquaye, L. S. Applications of Molecular Docking in Natural Products-Based Drug Discovery. *Scientific African* **2023**, *20*, e01593, <https://doi.org/10.1016/j.sciaf.2023.e01593>.
 28. Zochedh, A.; Chandran, K.; Priya, M.; Sultan, A. B.; Kathiresan, T. Molecular simulation of naringin combined with experimental elucidation–Pharmaceutical activity and Molecular docking against Breast cancer. *Journal of Molecular Structure* **2023**, *1285*, 135403, <https://doi.org/10.1016/j.molstruc.2023.135403>.
 29. Ferrari, I. V.; Di Mario, M. Prediction of physico-chemical property/Biological Activity and ADMET (absorption, distribution, mechanism, excretion, and toxicity) parameters of approved HIV Medications. *Int. J. Sci. Res. Biol. Sci.* **2022**, *9*, 76-86.
 30. Hassan, S. S. U.; Abbas, S. Q.; Ali, F.; Ishaq, M.; Bano, I.; Hassan, M.; Bungau, S. G. A Comprehensive in silico exploration of pharmacological properties, bioactivities, molecular docking, and anticancer potential of vieloplain F from *Xylopi* vielana Targeting B-Raf Kinase. *Molecules* **2022**, *27*, 917, <https://doi.org/10.3390/molecules27030917>.
 31. Priya, M.; Zochedh, A.; Arumugam, K.; Sultan, A. B. Quantum Chemical Investigation, Drug-Likeness and Molecular Docking Studies on Galangin as Alpha-Synuclein Regulator for the Treatment of Parkinson's Disease. *Chemistry Africa* **2023**, *6*, 287-309, <https://doi.org/10.1007/s42250-022-00508-z>.
 32. Zochedh, A.; Priya, M.; Shunmuganarayanan, A.; Thandavarayan, K.; Sultan, A. B. Investigation on structural, spectroscopic, DFT, biological activity and molecular docking simulation of essential oil Gamma-Terpinene. *Journal of Molecular Structure* **2022**, *1268*, 133651, <https://doi.org/10.1016/j.molstruc.2022.133651>.
 33. Chandran, K.; Shane, D. I.; Zochedh, A.; Sultan, A. B.; Kathiresan, T. Docking simulation and ADMET prediction based investigation on the phytochemical constituents of Noni (*Morinda citrifolia*) fruit as a potential anticancer drug. *In Silico Pharmacol.* **2022**, *10*, 14, <https://doi.org/10.1007/s40203-022-00130-4>.
 34. Priya, M.; Zochedh, A.; Chandran, K.; Arumugam, K.; Banu, S.; Chakaravarthy, C.; Sultan, A. B. Computer-Aided Analysis of Biochanin-A as a Potential Breast Cancer Drug Based on DFT, Molecular Docking, and Pharmacokinetic Studies. *Letters in Applied NanoBioScience* **2022**, *12*, 165, <https://doi.org/10.33263/LIANBS124.165>.
 35. Zochedh, A.; Shunmuganarayanan, A.; Sultan, A. B. Conformational fidelity and hydrogen bond associability of L-histidine with sulfamate anion studied through XRD, quantum chemical, spectroscopic and molecular docking simulation as a cdk-4 inhibitor against retinoblastoma. *Journal of Molecular Structure* **2023**, *1274*, 134402, <https://doi.org/10.1016/j.molstruc.2022.134402>.
 36. Novena, L. M.; Athimoolam, S.; Anitha, R.; Bahadur, S. A. Synthesis, crystal structure, hirshfeld surface analysis, spectral and quantum chemical studies of pharmaceutical cocrystals of a bronchodilator drug (Theophylline). *Journal of Molecular Structure* **2022**, *1249*, 131585, <https://doi.org/10.1016/j.molstruc.2021.131585>.
 37. Thangarasu, S.; Siva, V.; Kannan, S.; Bahadur, S. A.; Athimoolam, S. Polymorphism in Chloride Salt of m-Nitroaniline: Structural, Spectroscopic, Thermal, Molecular Docking, Biological, and Quantum Chemical Computational Investigation. *Polycyclic Aromatic Compounds* **2022**, *43*, 1-18, <https://doi.org/10.1080/10406638.2022.2130374>.
 38. Sukumaran, S.; Zochedh, A.; Viswanathan, T. M.; Sultan, A. B.; Kathiresan, T. Theoretical Investigation of 5-Fluorouracil and Tamoxifen Complex–Structural, Spectrum, DFT, ADMET and Docking Simulation. *Polycyclic Aromatic Compounds* **2023**, *43*, 1-18, <https://doi.org/10.1080/10406638.2022.2164018>.
 39. Viswanathan, T. M.; Zochedh, A.; Chandran, K.; Sukumaran, S.; Sultan, A. B.; Kathiresan, T. Investigation of Guanidine–Curcumin Complex based on Quantum Chemicals, Pharmacokinetics and Molecular Docking

Simulation against Breast Cancer: A Theoretical Approach. *Asian Journal of Chemistry* **2023**, *35*, 1189-1198, <https://doi.org/10.14233/ajchem.2023.27805>.

Publisher's Note & Disclaimer

The statements, opinions, and data presented in this publication are solely those of the individual author(s) and contributor(s) and do not necessarily reflect the views of the publisher and/or the editor(s). The publisher and/or the editor(s) disclaim any responsibility for the accuracy, completeness, or reliability of the content. Neither the publisher nor the editor(s) assume any legal liability for any errors, omissions, or consequences arising from the use of the information presented in this publication. Furthermore, the publisher and/or the editor(s) disclaim any liability for any injury, damage, or loss to persons or property that may result from the use of any ideas, methods, instructions, or products mentioned in the content. Readers are encouraged to independently verify any information before relying on it, and the publisher assumes no responsibility for any consequences arising from the use of materials contained in this publication.